Hydrodynamic slip boundary condition at chemically patterned surfaces: A continuum deduction from molecular dynamics

Tiezheng Qian and Xiao-Ping Wang
Department of Mathematics, Hong Kong University of Science and Technology, Clear Water Bay, Kowloon, Hong Kong, China

Ping Sheng
Department of Physics and Institute of Nano Science and Technology, Hong Kong University of Science and Technology, Clear Water Bay, Kowloon, Hong Kong, China

(Received 10 February 2005; revised manuscript received 2 June 2005; published 18 August 2005)

We investigate the slip boundary condition for flows past a chemically patterned surface. Molecular dynamics simulations show that fluid forces and stresses vary laterally along the patterned surface. A subtraction scheme is developed to verify the validity of the Navier slip boundary condition, locally, for the patterned surface. A continuum hydrodynamic model is formulated using the Navier-Stokes equation and the Navier boundary condition, with a slip length varying along the patterned surface. Steady-state velocity fields from continuum calculations are in quantitative agreement with those from molecular simulations.

DOI: 10.1103/PhysRevE.72.022501 PACS number(s): 83.50.Lh, 83.10.Rs, 83.50.Rp

Recently developed techniques of microfluidics [1] have generated great interest in further miniaturization towards nanofluidics [2]. Theoretical and experimental studies of confined fluids have shown that the slip boundary condition at the fluid-solid interface can strongly influence the flow behavior as the system size approaches nanoscale [3]. Molecular dynamics (MD) studies of slip have focused on single-phase flow [4–8] and miscible [9,10] and immiscible [11–13] two-phase flows past homogeneous surfaces. On the other hand, chemically patterned surfaces have generated interest in novel control of flow in micro- and nanofluidics [14,15]. In particular, slip flow past nanopatterned surfaces has been investigated using both MD and continuum simulations [16–20].

In this paper we study the slip boundary condition for single-phase flow past a chemically patterned surface. The validity of the Navier slip boundary condition, locally, is demonstrated. Continuum calculations are carried out using the Navier-Stokes equation and the Navier boundary condition (NBC), with a slip length varying along the patterned surface. Continuum steady-state velocity fields are in quantitative agreement with those from MD simulations. Continuum calculations show that when the pattern period is sufficiently small compared to the slip length, the solid surface appears to be approximately homogeneous, with an effective slip length tunable by surface patterning.

MD simulations have been carried out for Couette flow between two solid planar walls parallel to the xy plane, one with a homogeneous surface at $z=H$ and the other a patterned surface at $z=0$. The Couette flow is generated by fixing the lower wall and moving the upper wall at a constant speed V in the x direction. Periodic boundary conditions are imposed in the x and y directions. Interaction between fluid molecules of distance r is modeled by a Lennard-Jones (LJ) potential $U_{ff}(r)=4\epsilon[(\sigma/r)^{12}-(\sigma/r)^{6}]$, where ϵ is the energy scale and σ the range scale. The average number density for the fluid is set at $\rho=0.81\sigma^{-3}$. The temperature is maintained at $1.4\epsilon/k_B$. Each wall is constructed by two [001] planes of an fcc lattice, with each wall molecule attached to a lattice site by a harmonic spring. The mass of the wall molecule equals that of the fluid molecule m. The number density of the wall equals $\rho_w=1.86\sigma^{-3}$. The fluid-solid interaction is modeled by a modified LJ potential $U_{fs}(r)=4\epsilon_{fs}[(\sigma_{fs}/r)^{12}-\delta_{fs}(\sigma_{fs}/r)^{6}]$, with the energy and range parameters given by $\epsilon_{fs}=1.16\epsilon$ and $\sigma_{fs}=1.04\sigma$, and a dimensionless parameter δ_{fs} for adjusting the wetting property of the fluid. The lower solid surface is patterned, and the patterning is modeled by the oscillating parameter [21]: $\delta_{fs}(x)=\delta_0+\delta_1\cos(2\pi x/P)$, where x is the x-coordinate of the wall molecule, δ_0 is a constant, δ_1 is the oscillation amplitude for δ_{fs}, and P is the oscillation period, set to be larger than 10σ. The upper solid surface is homogeneous, where the fluid-solid interaction has a constant δ_{fs} equaling δ_0. We use $\delta_0=1$ and $\delta_1=0.3$. The fluid-solid interaction potential U_{fs} is cut off at $r_c=2.2\sigma$. The confined fluid measures H along z and the system dimensions along x and y are L and 6.8σ. The MD results are obtained for $V=0$ and $0.25\sqrt{\epsilon/m}$, $H=13.6\sigma$, and $L=54.5\sigma$, with $L=P$ or $2P$.

We measure five quantities: G_x^w, the tangential wall force per unit area exerted by the wall on the fluid molecules in a horizontal layer; σ_{xx} and σ_{zx}, the xx and zx components of the fluid stress tensor; and v_x and v_z, the x and z components of the fluid velocity. As reference quantities, we also measure G_x^{w0}, σ_{xx}^0, and σ_{zx}^0 in the static ($V=0$) state. Here the superscript "0" denotes the static quantities. Spatial resolution along the x and z directions is obtained by evenly dividing the measurement region into bins, each $\Delta x=0.85\sigma$ by $\Delta z=0.85\sigma$. Static equilibrium-state ($V=0$) and dynamic steady-state ($V\neq 0$) quantities are obtained from time average over $5\times 10^5\tau$ or longer where $\tau=\sqrt{m\sigma^2/\epsilon}$.

In the static state, various fluid forces and stresses vary along the patterned surface. The nonuniform static state forms a microscopic background upon which hydrodynamic variations are generated when the fluid is sheared. To obtain

a hydrodynamic quantity, the static part needs to be subtracted from the corresponding dynamic quantity:

$$\tilde{Q} = Q_D - Q_S, \tag{1}$$

where Q_S is a static (reference) quantity, Q_D the corresponding dynamic quantity, and the overtilde denotes the hydrodynamic quantity. Physically, the characteristic variation magnitude of $\tilde{Q}$ should be much smaller than that of Q_D and Q_S. Therefore, in deducing a continuum relation, if a hydrodynamic quantity $\tilde{Q}$ is to be used, then it can by no means be replaced by a dynamic quantity Q_D, without subtracting the static part.

The hydrodynamic tangential force balance in the boundary layer between $z=0$ and $z=\Delta z$ is

$$\tilde{G}_x^w(x,\Delta z/2) + \tilde{G}_x^f(x,\Delta z/2) = 0, \tag{2}$$

with the hydrodynamic tangential fluid force

$$\tilde{G}_x^f(x,\Delta z/2) = \partial_x \int_0^{\Delta z} dz \tilde{\sigma}_{xx}(x,z) + \tilde{\sigma}_{zx}(x,\Delta z). \tag{3}$$

This integrated form is necessary because the tangential wall force is distributed within a finite distance from the wall. Beyond the boundary layer, the hydrodynamic tangential wall force $\tilde{G}_x^w$ vanishes. The short-range nature of $\tilde{G}_x^w$ is due to the fact that $\tilde{G}_x^w$ solely arises from the "roughness" of wall potential [5]. Hereafter we use $\tilde{G}_x^w(x)[=\tilde{G}_x^w(x,\Delta z/2)]$ to denote the total hydrodynamic tangential wall force. We take the sharp boundary limit by letting $\tilde{G}_x^w$ strictly concentrate at $z=0$. This leads to $\tilde{G}_x^f(x,\Delta z/2)=\tilde{\sigma}_{zx}(x,0^+)$. Hereafter we use $\tilde{G}_x^f(x)[=\tilde{G}_x^f(x,\Delta z/2)]$ to denote the hydrodynamic tangential fluid force. It follows that

$$\tilde{G}_x^f(x) = \tilde{\sigma}_{zx}(x,0^+) = -\tilde{G}_x^w(x), \tag{4}$$

from which a slip boundary condition will be obtained.

The hydrodynamic viscous coupling between the fluid and solid is described by the Navier slip model:

$$\tilde{G}_x^w(x) = -\beta(x) v_x^{slip}(x), \tag{5}$$

where $\beta(x)$ is the local slip coefficient and the slip velocity v_x^{slip} is the boundary-layer tangential fluid velocity relative to the wall, i.e., $v_x^{slip}=v_x$ at the lower surface or $v_x^{slip}=v_x-V$ at the upper surface. The Navier slip model has been verified by many MD studies, but mostly for homogeneous solid surfaces only [4–7]. For patterned surfaces, the local nature of the Navier model can be better revealed. In particular, the *local* coupling constant β should depend on x through the parameter $\delta_{fs}(x)$ in potential U_{fs}:

$$\beta(x) = \beta(\delta_{fs}(x)), \tag{6}$$

where β as a function of δ_{fs}, denoted by $\beta(\delta_{fs})$, relates a microscopic interaction parameter and a hydrodynamic slip coefficient.

To verify Eq. (6), independent MD simulations have been carried out for Couette flows between two identical homogeneous solid surfaces, using fluid-solid interaction potentials

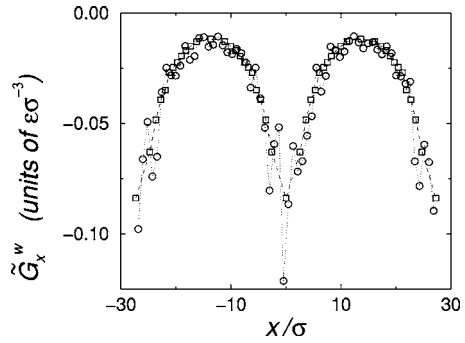

FIG. 1. Hydrodynamic tangential wall force $\tilde{G}_x^w(x)$ at the lower fluid-solid interface. The circles denote $\tilde{G}_x^w(x)$ directly measured in the MD simulation; the squares denote $\tilde{G}_x^w(x)$ calculated from $\beta(x)$ and the measured $v_x^{slip}(x)$.

with a constant δ_{fs}. For each particular value of δ_{fs}, the slip coefficient β can be measured. The functional dependence of β on δ_{fs}, $\beta(\delta_{fs})$, has been numerically obtained by scanning a set of values for δ_{fs}. Substituting $\delta_{fs}(x)$ into $\beta(\delta_{fs})$ then yields $\beta(x)$ for the patterned surface. Using this $\beta(x)$ and the slip velocity profile $v_x^{slip}(x)$ directly measured in the MD simulation, we calculate $\tilde{G}_x^w(x)$ at the patterned surface according to Eq. (5), shown in Fig. 1 with a comparison to the measured $\tilde{G}_x^w(x)$. The good agreement clearly verifies the local Navier slip model expressed by Eqs. (5) and (6). Of course, the local dependence of β on δ_{fs} is not without limit. Physically, to validate Eq. (6) for $\beta(x)$ in Eq. (5), the lateral variation of δ_{fs} must be slow. In fact, the disagreement between MD and continuum results was observed for pattern period approaching a molecular scale [20].

Far away from the solid surface, the momentum transport is described by the Navier-Stokes equation

$$\rho\left[\frac{\partial \mathbf{v}}{\partial t} + (\mathbf{v}\cdot\boldsymbol{\nabla})\mathbf{v}\right] = -\boldsymbol{\nabla} p + \eta\boldsymbol{\nabla}^2\mathbf{v}, \tag{7}$$

where the viscosity $\eta=2.1\sqrt{\epsilon m}/\sigma^2$ has been determined by MD measurements. Close to the rigid wall, however, the fluid density shows a short-range oscillation along the sur-

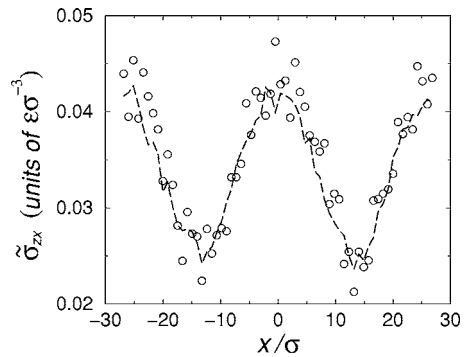

FIG. 2. Hydrodynamic tangential stress $\tilde{\sigma}_{zx}(x,z)$ at $z=2\Delta z$, plotted as a function of x. The circles denote $\sigma_{zx}(x,2\Delta z)-\sigma_{zx}^0(x,2\Delta z)$; the dashed line denotes $\eta(\partial_z v_x+\partial_x v_z)$ calculated from the MD flow field, with $\eta=2.3\sqrt{\epsilon m}/\sigma^2$ to achieve the best agreement.

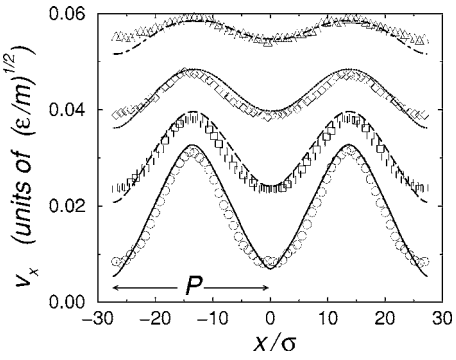

FIG. 3. v_x plotted as a function of x for four z levels close to the lower wall of sinusoidal fluid-solid interaction. The symbols denote the MD data and the lines represent the corresponding continuum results, obtained for a system of $H=13.6\sigma$, $L=2P=54.4\sigma$, and $V=0.25\sqrt{\epsilon/m}$. The four z levels are at $z=0.425\sigma$ (circles and solid line), 1.275σ (squares and dashed line), 2.125σ (diamonds and dotted line), and 2.975σ (triangles and dash-dotted line).

face normal z across a few molecular layers, in addition to a lateral oscillation along x imposed by the surface pattern. We proceed using a constant viscosity throughout the fluid space. The hydrodynamic tangential stress $\tilde{\sigma}_{zx}(x,z)$ has been measured at $z=2\Delta z$ where density oscillation is $\approx 10\%$, and then compared to that calculated from the Newtonian relation $\eta(\partial_z v_x+\partial_x v_z)$ using the MD measured velocity field (see Fig. 2). The overall agreement is satisfactory. Combining Eqs. (4)–(6) with the Newtonian relation for $\tilde{\sigma}_{zx}$ at the solid surface yields the NBC

$$\beta(\delta_{fs}(x))v_x=\eta\partial_z v_x, \tag{8}$$

with a local slip coefficient $\beta(\delta_{fs}(x))$. The local slip length is defined as $l_s(x)=\eta/\beta(\delta_{fs}(x))$. Continuum calculations involve six parameters, none adjustable: the system dimensions L and H, the shearing speed V, the fluid density ρ, the viscosity η, and the slip coefficient β (as a function of δ_{fs}).

The continuum and MD results agree quantitatively. Figures 3 and 4 show the periodic v_x profiles close to the lower wall, for sinusoidal and stepwise $\delta_{fs}(x)$'s in $U_{fs}(r)$, respectively. The latter case corresponds to the transverse case studied in Ref. [20]. In the first period $-P/2\leqslant x<P/2$, $\delta_{fs}(x)=\delta_0-\delta_1$ for $-P/4\leqslant x<P/4$ or $\delta_0+\delta_1$ elsewhere. The small discrepancies may be attributed to the small H, the nonuniform boundary-layer fluid, and the fast variation of δ_{fs}.

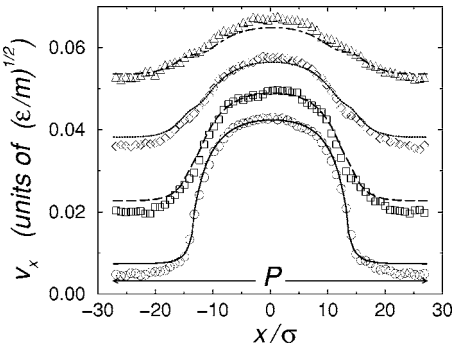

FIG. 4. v_x plotted as a function of x for four z levels close to the lower wall of stepwise fluid-solid interaction. The symbols denote the MD data and the lines represent the corresponding continuum results, obtained for a system of $H=13.6\sigma$, $L=P=54.4\sigma$, and $V=0.25\sqrt{\epsilon/m}$. The four z levels are at $z=0.425\sigma$ (circles and solid line), 1.275σ (squares and dashed line), 2.125σ (diamonds and dotted line), and 2.975σ (triangles and dash-dotted line).

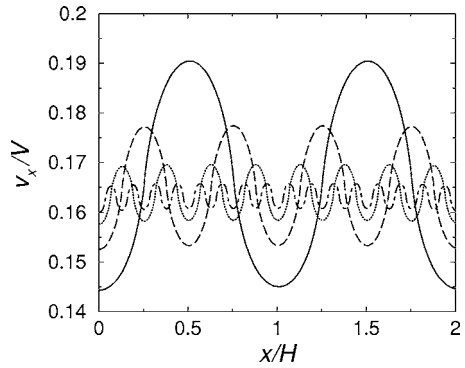

FIG. 5. Slip profiles at differently patterned solid surfaces. The pattern period $P=w_A+w_B$ varies from H to $H/8$, with equal stripe widths ($w_A=w_B$). The solid line is for $P/H=1$, the dashed line for $P/H=1/2$, the dotted line for $P/H=1/4$, and the dash-dotted line for $P/H=1/8$.

More continuum hydrodynamic calculations have been carried out for viscous flow with small Reynolds numbers $\mathrm{Re}=\rho VH/\eta\approx 1$. Analytical and numerical results have been obtained for Stokes flow satisfying mixed slip conditions, and the concept of effective slip length has been introduced for different flow geometries with various patterned surfaces [16,17,19,20]. Our results here show essentially the same physics. We consider a patterned surface composed of a periodic array of stripes parallel to the y axis, each of type A or B, arranged according to $\cdots ABABAB\cdots$ to realize the periodicity along the x direction. The continuum model uses two different slip lengths l_{sA} and l_{sB} for A and B stripes, respectively, and the surface pattern is continuously varied. The scaled steady-state velocity fields, $\mathbf{v}(x/H,z/H)/V$, are controlled by the dimensionless parameters l_{sA}/H, l_{sB}/H, w_A/H, and w_B/H, where w_A and w_B are the widths of A and B stripes.

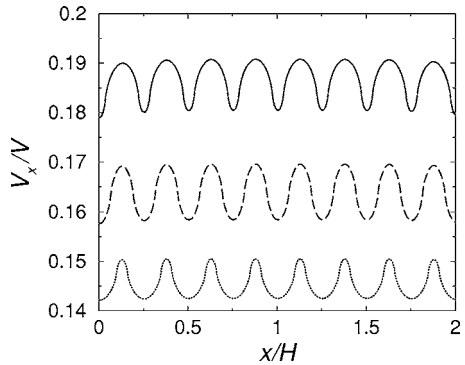

FIG. 6. Slip profiles at differently patterned solid surfaces. The pattern period $P=w_A+w_B$ equals $H/4$, with w_A/w_B varying from $1/3$ (solid line) to 1 (dashed line) and to 3 (dotted line).

Steady-state slip profiles are obtained for six differently patterned surfaces with $l_{sA}/H=0.147$ and $l_{sB}/H=0.441$. Figure 5 shows that the slip velocity becomes less oscillatory in magnitude as the pattern period P is decreased. Therefore a solid surface patterned with a sufficiently small period appears to be homogeneous. The nearly uniform slip velocity can be used to define an effective slip length l_s^{eff}, given by $l_s^{eff}/H=v_x^{ave}/(V-v_x^{ave})$ for the Couette flow. The data in Fig. 5 yield $l_s^{eff}/H=0.196$. For small period P, the effective slip length can be further tuned by varying the ratio of the two stripe widths. Figure 6 shows that by fixing P/H at 1/4 and increasing the proportion of the A stripes, the average amount of slip is appreciably reduced. So l_s^{eff} decreases with the increasing proportion of the A stripes.

In summary, for single-phase flow past a chemically patterned surface, the validity of the NBC has been verified. A continuum hydrodynamic model has been formulated, yielding steady-state flow fields in quantitative agreement with MD results. It is also shown that an effective slip length can be realized and tuned by surface patterning.

This work was partially supported by Hong Kong RGC DAG 03/04.SC21. We would like to thank Professor W. E and Dr. W. Ren for helpful discussions.

[1] G. M. Whitesides and A. D. Stroock, Phys. Today **54**, 42 (2001).
[2] H. A. Stone, A. D. Stroock, and A. Ajdari, Annu. Rev. Fluid Mech. **36**, 381 (2004).
[3] S. Granick, Y. X. Zhu, and H. Lee, Nat. Mater. **2**, 221 (2003).
[4] P. A. Thompson and M. O. Robbins, Phys. Rev. A **41**, 6830 (1990).
[5] P. A. Thompson and S. M. Troian, Nature (London) **389**, 360 (1997).
[6] J.-L. Barrat and L. Bocquet, Phys. Rev. Lett. **82**, 4671 (1999).
[7] M. Cieplak, J. Koplik, and J. R. Banavar, Phys. Rev. Lett. **86**, 803 (2001).
[8] V. P. Sokhan, D. Nicholson, and N. Quirke, J. Chem. Phys. **117**, 8531 (2002).
[9] J. Koplik and J. R. Banavar, Phys. Rev. Lett. **80**, 5125 (1998).
[10] C. Denniston and M. O. Robbins, Phys. Rev. Lett. **87**, 178302 (2001).
[11] J. Koplik, J. R. Banavar, and J. F. Willemsen, Phys. Rev. Lett. **60**, 1282 (1988).
[12] P. A. Thompson and M. O. Robbins, Phys. Rev. Lett. **63**, 766 (1989).
[13] T. Z. Qian, X. P. Wang, and P. Sheng, Phys. Rev. Lett. **93**, 094501 (2004).
[14] H. Gau, S. Herminghaus, P. Lenz, and R. Lipowsky, Science **283**, 46 (1999).
[15] L. Kondic and J. Diez, Phys. Rev. E **65**, 045301 (2002).
[16] J. R. Philip, Z. Angew. Math. Phys. **23**, 960 (1972).
[17] E. Lauga and H. A. Stone, J. Fluid Mech. **489**, 55 (2003).
[18] C. Cottin-Bizonne, J.-L. Barrat, L. Bocquet, and E. Charlaix, Nat. Mater. **2**, 237 (2003).
[19] C. Cottin-Bizonne, C. Barentin, E. Charlaix, L. Bocquet, and J.-L. Barrat, Eur. Phys. J. E **15**, 427 (2004).
[20] N. V. Priezjev, A. A. Darhuber, and S. M. Troian, Phys. Rev. E **71**, 041608 (2005).
[21] W. Ren and W. E, J. Comput. Phys. **204**, 1 (2005).